Anatomies, vascular architectures, and mechanics underlying the leaf size-stem size spectrum in 42 Neotropical tree species

Sébastien Levionnois, Camille Salmon, Tancrède Alméras, Bruno Clair, Camille Ziegler, Sabrina Coste, Clement Stahl, Andrés González-Melo, Christine Heinz, Patrick Heuret

Anatomies, vascular architectures, and mechanics underlying the leaf size-stem size spectrum in 42 Neotropical tree species

Sébastien Levionnois[1,2*] (ORCID: 0000-0002-7217-9762), Camille Salmon[2], Tancrède Alméras[3] (ORCID: 0000-0002-2843-5466), Bruno Clair[3] (ORCID: 0000-0002-4093-9034), Camille Ziegler[1,4] (ORCID: 0000-0002-0855-1347), Sabrina Coste[1] (ORCID: 0000-0003-3948-4375), Clément Stahl[1] (ORCID: 0000-0001-5411-1169), Andrés González-Melo[5] (ORCID: 0000-0003-0069-456X), Christine Heinz[2], Patrick Heuret[2*] (ORCID: 0000-0002-7956-0451)

[1]UMR EcoFoG, AgroParisTech, CIRAD, CNRS, INRAE, Université des Antilles, Université de Guyane, 97310 Kourou, France.

[2]UMR AMAP, Université de Montpellier, CIRAD, CNRS, INRAE, IRD, Université de Montpellier, 34000 Montpellier, France.

[3]LMGC, CNRS, Université de Montpellier, 34090 Montpellier, France.

[4]UMR SILVA, INRAE, Université de Lorraine, 54000 Nancy, France.

[5]Universidad del Rosario, 110111 Bogotá, Colombia.

*Authors for correspondence:

Sébastien Levionnois, PhD

Postal

UMR AMAP, TA 1-51/PS2 Boulevard de la Lironde

34398 Montpellier Cedex 5, France

Tel: +33 760 26 73 83

Email: sebastien.levionnois.pro@gmail.com

Patrick Heuret, PhD

Postal adress: UMR AMAP, TA 1-51/PS2 Boulevard de la Lironde

34398 Montpellier Cedex 5, France

Tel: +33 467 61 55 14

Email: patrick.heuret@inrae.fr

HIGHLIGHT

Water supply and mechanical stability remain proportional to shoot leaf area because of allometric scaling of vessel diameter and stem length with shoot size across 42 Neotropical tree species, deviating from theoretical isometry with shoot size.

ABSTRACT

The leaf size-stem size spectrum is one of the main dimensions of plant ecological strategies. Yet the anatomical, mechanical, and hydraulic implications of small vs. large shoots are still poorly understood. We investigated 42 tropical rainforest tree species in French Guiana, with a wide range of leaf areas at the shoot level. We quantified the scaling of hydraulic and mechanical constraints with shoot size estimated as the water potential difference $\Delta\Psi$ and the bending angle $\Delta\Phi$, respectively. We investigated how anatomical tissue area, flexural stiffness and xylem vascular architecture affect such scaling by deviating (or not) from theoretical isometry with shoot size variation. Vessel diameter and conductive path length were found to be allometrically related to shoot size, thereby explaining the independence between $\Delta\Psi$ and shoot size. Leaf mass per area, stem length, and the modulus of elasticity were allometrically related with shoot size, explaining the independence between $\Delta\Phi$ and shoot size. Our study also shows that the maintenance of both water supply and mechanical stability across the shoot size range are not in conflict.

Key words: allometry, anatomy, axial vessel widening, leaf size spectrum, mechanics, scaling, shoot, water supply**.**

INTRODUCTION

The leaf size-stem size (LS-SS) spectrum is considered as one of the main dimensions of plant ecological strategies (Westoby *et al.*, 2002; Westoby and Wright, 2003; Lauri, 2019). Several similar concepts have been proposed to study the LS-SS spectrum: Corner's rules (Corner, 1949; Hallé *et al.*, 1978; White, 1983*a*,*b*; Brouat *et al.*, 1998; Ackerly and Donoghue, 1998; Olson *et al.*, 2018), leaf-stem allometry (Brouat and McKey, 2001; Normand *et al.*, 2008; Fan *et al.*, 2017), the leaf size-twig size spectrum (Westoby and Wright, 2003; Sun *et al.*, 2006), and the leptocaulis-pachycaulis spectrum (Corner, 1949; Hallé *et al.*, 1978). A central question underlying these concepts relates to the relationships among morphological traits, between isometry and allometry (Brouat *et al.*, 1998). Isometry refers to a strict relationship of proportionality, whereas allometry refers to different rates of variation usually described by a power function between two traits, with two distinguishable forms of allometry. For $Y \propto X^b$, hyper-allometry refers to a disproportionate *increase* in Y in comparison to X ($b > 1$), while hypo-allometry refers to a disproportionate *decrease* in Y in comparison to X ($b < 1$; Shingleton, 2010). Identifying whether trait scaling is allometric or isometric is a priority, as this may reflect diverging sizing of constraints (e.g. hydraulic tension, mechanical stress, carbon economy) with organ or organism size, and further sheds light on the selective value of large vs. small organs or organisms in a given environment. Regarding the LS-SS spectrum, beyond testing isometry vs. allometry, such constraints are rarely quantified or modelled, which further hampers the understanding of the selective value of large vs. small leaves, and the determination of what drives the wide range of leaf sizes across the world (Westoby *et al.*, 2002; Wright *et al.*, 2017).

The 'leaf area ∝ stem cross-sectional area' scaling (hereafter abbreviated respectively, A_{leaf} and A_{stem}) is the relationship most frequently investigated in the LS-SS framework. Most studies support hyper-allometric scaling of $A_{\text{leaf}} \propto A_{\text{stem}}$ at the interspecific level (Brouat and McKey, 2001; Westoby and Wright, 2003; Preston and Ackerly, 2003; Sun *et al.*, 2006; Normand *et al.*, 2008; Xiang *et al.*, 2009; Yang *et al.*, 2009; Liu *et al.*, 2010; Yan *et al.*, 2013; Osada *et al.*, 2015), but two studies support isometry (Brouat *et al.*, 1998; Fan *et al.*, 2017). If hyper-allometry is the rule for the $A_{\text{leaf}} \propto A_{\text{stem}}$ scaling, this suggests large shoots would have a higher leaf area per stem cross-sectional area than small shoots. In this case, the shoot is not homothetic, i.e. leaf geometry depends on leaf size. This allometric scaling may reflect diverging constraints in large vs. small leaves, which may be buffered by different geometries, or which may be reflected in lower and higher performance, and further affect the selective value of large- vs. small-leaves. However, to our knowledge, such constraints have never been formalised along the LS-SS spectrum. Here, we propose such a formalism, for both a hydraulic (water transport) and a mechanical function (flexural support). This formalism may help understand if variation in geometry, i.e. allometric scaling between traits, is a response to hydraulic or mechanical constraints across a broad range of leaf sizes.

Regarding water supply, it can be assumed that a major constraint when increasing organ size is the difference in water potential, as a too large difference could lead to xylem embolism and plant dehydration (Tyree and Sperry, 1989; Tyree and Zimmermann, 2002; Cruiziat *et al.*, 2002), but a too small difference could strongly reduce water flow. Differences in plant water potential have already been successfully modelled following Darcy's law (Whitehead *et al.*, 1984; Sperry *et al.*, 1998; Martin- StPaul *et al.*, 2017). The model we present is directly derived from this framework. We can therefore write:

$$(1)\ \Delta\Psi = \Psi_{stem} - \Psi_{leaf} \sim \frac{A_{leaf} \times L_{path}}{K_s \times A_{xylem}} \sim \frac{A_{leaf} \times L_{path}}{VD \times {D_h}^4 \times A_{xylem}}$$

where Ψ_{stem} and Ψ_{leaf} are the water potentials (MPa) in stems and leaves, respectively (or at the base and the tip of the conductive path, respectively), A_{leaf} is the total shoot leaf area supplied with water (m²), L_{path} is the length of the conductive path (cm), K_s is xylem-specific conductivity (kg m^{-1} MPa^{-1} s^{-1}), A_{xylem} is the xylem surface area (mm²), VD is the xylem vessel density (mm^{-2}), and D_h is the vessel mean hydraulic diameter (µm). Note that we assume proportionality, and not equality, so that factors such as water viscosity, vapour pressure deficit or leaf conductance are neglected in this formulation.

We can analyse the dependence of all these factors on the stem diameter at the base of the shoot D_{stem} (mm), after log transformation. The equation (1) can then be decomposed as:

$$(2)\ P(\Delta\Psi) = P(A_{leaf}) + P(L_{path}) - P(VD) - 4 \times P(D_h) - P(A_{xylem})$$

where $P(X)$ is the slope of the $\log(X) \propto \log(D_{stem})$ relationship. If we assume isometric scaling of all morphological factors (A_{leaf}, L_p, A_{xylem}) with D_{stem}, but no vascular change (VD, D_h), then $P(A_{leaf}) = 2$, $P(L_{path}) = 1$, $P(\mathrm{VD}) = 0$, $P(D_h) = 0$, and $P(A_{xylem}) = 2$. To sum up, $P(\Delta\Psi) = 1$, indicates that $\Delta\Psi$ increases with size under this scenario and suggests shoots with large leaves are disadvantaged with respect to water transport. Therefore, as $A_{leaf} \propto A_{stem}$ scaling has been shown to be isometric, and even hyper-allometric (see references above), compensation must be achieved through these factors to allow proportionate water supply across species with large vs. small leaves. For instance, $P(D_h) = 0.25$, leading to widening of axial vessels, would compensate for the increase in hydraulic resistance (i.e. increasing $\Delta\Psi$), in agreement with already proposed hydraulic optimality models (West *et al.*, 1999;

Anfodillo *et al.*, 2013). Indeed, axial vessel widening is a well-known phenomenon at the stem (Anfodillo *et al.*, 2006; Olson *et al.*, 2014) and leaf level (Lechthaler *et al.*, 2019; Levionnois *et al.*, 2020), but has been poorly investigated at the shoot level or in tropical rainforest trees.

Regarding mechanical support, it can be assumed that a major constraint with increasing organ size is minimising the bending angle which causes stem deflection and reduces light interception, or may even cause the stem to rupture. Based on simple theory, we can model the stem bending angle as:

$$(3)\ \Delta\Phi \sim \frac{LMA \times A_{leaf} \times {L_{stem}}^2}{MOE \times I}$$

where $\Delta\Phi$ is the difference in bending angle between the tip and the base of the shoot stem (hereafter simplified to 'bending angle'), LMA is the leaf mass per leaf area (g m^{-2}), A_{leaf} is the shoot leaf area (cm^2), L_{stem} is the stem length (cm), MOE is the modulus of elasticity (kN mm^{-2}), and I the second moment of area (mm^4). Note also that L_{stem} differs from L_p in the above hydraulic model (see material and methods).

We can analyse the dependence of all these factors on the stem diameter at the base of the shoot D_{stem} (mm), after log transformation. Equation (3) can then be decomposed as:

$$(4)\ P(\Delta\Phi) = P(LMA) + P(A_{leaf}) + 2 \times P(L_{stem}) - P(MOE) - P(I)$$

where $P(X)$ is the slope of the $\log(X) \propto \log(D_{stem})$ relationship. If we assume isometric scaling of all factors with D_{stem}, then $P(\text{LMA}) = 1$ (assuming a proportional increase in leaf thickness), $P(A_{leaf}) = 2$, $P(L_{stem}) = 1$, $P(\text{MOE}) = 0$, and $P(I) = 4$. To sum up, $P(\Delta\Phi) = 1$, indicates that $\Delta\Phi$ increases with size under this scenario thereby suggesting that shoots with larger leaves are disadvantaged regarding stem flexural stiffness. Therefore, as $A_{leaf} \propto A_{stem}$ scaling has been shown to be isometric, and even hyper-allometric (see references above), mechanical compensation must be achieved through these factors to allow proportionate stem flexural stiffness across species with large vs. small leaves. For instance, this could be achieved through by reducing L_{stem}, or by increasing MOE. However, Olson *et al.* (2018*a*) demonstrated that species with large leaves and stems require low stem density, and therefore exhibit low MOE. However, to our knowledge, no study has jointly analysed LS-SS scaling and its main mechanical parameters (MOE, *I*) in the light of the mechanical constraint determined by $\Delta\Phi$.

As xylem fulfils different functions including mechanical support, water conduction, and water and photosynthetic storage, a hydraulic-mechanic trade-off emerges at the level of the xylem (Baas *et al.*, 2004; Chave *et al.*, 2009; Lachenbruch and McCulloh, 2014;

Bittencourt *et al.*, 2016). Indeed, the storage and transport of large volumes of water requires large vessels and a large parenchyma lumen fractions, while mechanical strength requires large fibre and large fibre wall fractions, leading to a conflict for space. It is not known if this trade-off holds true at the stem or shoot level. A recent study suggested this is the case (Fan *et al.*, 2017), but only based on measurements of material properties (MOE and K_s), and not taking the effect of the overall structure (I and xylem area) into account. What is more, all the parameters that determine overall flexural performance (MOE and I) and the overall water supply performance (K_s and xylem area) have never been analysed together, to properly understand if mechanical support and water supply are in conflict at the shoot level.

We quantified the scaling of the LS-SS spectrum, based on the $A_{leaf} \propto A_{stem}$ scaling, in a wide range of shoot leaf areas. We took advantage of the high morphological diversity in leaf area in Amazon rainforest trees in French Guiana to examine a wide range of leaf and stem sizes across 42 species. We incorporated vascular and theoretical hydraulic traits as well as mechanical traits, at the shoot level (i.e., on a single unbranched stem with its leaves), based on two sets of shoot samples, respectively. We specifically addressed the following questions:

- What are the adjustments (A_{leaf}, L_p, VD, D_h, A_{xylem}), i.e., deviation from expected isometry (Eq. 2 and 4) that mitigate the hydraulic constraint quantified as the difference in leaf-stem water potential $\Delta\Psi$ with increasing shoot size?
- What are the adjustments (LMA, A_{leaf}, L_{stem}, MOE, I) that mitigate the mechanical constraint quantified as the bending angle $\Delta\Phi$ that occurs with increasing shoot size?
- Are mechanical support and water supply in conflict along the LS-SS spectrum at the shoot level?

MATERIALS AND METHODS

Study site, species, and plant material

The experiment was conducted at the Paracou experimental station (https://paracou.cirad.fr/website; 5°16’26’’N, 52°55’26’’W), French Guiana, located in a lowland tropical rainforest (Gourlet-Fleury *et al.*, 2004). The tropical climate of French Guiana is highly seasonal due to the north-south movement of the Inter-Tropical Convergence Zone. The mean (± SE) annual air temperature is 25.7 °C ± 0.1°C and the mean precipitation (from 2004 to 2014) was 3,102 mm ± 70 mm (Aguilos *et al.*, 2019). The dry season lasts from mid-August to mid-November, during which rainfall is < 100 mm month^{-1}.

Adult trees of 42 species representing marked phylogenetic diversity (Magnolid, Rosid, and Asterid clades) were sampled to account for morphological and anatomical diversity (Table S1). Mainly canopy dominant or co-dominant, adult trees exposed to the sun were sampled. However, three shade tolerant species were part of the mid storey. One shoot per tree was sampled. In the context of our study, a shoot is defined as the single unbranched stem supporting the most leaves, with no missing or damaged leaves between the youngest leaf and the oldest leaf (Fig. 1). Shoots were cut at the base of the internode supporting the last, oldest leaf. In this way, the quantity of wood and vessels at the base of the shoot can be associated with a precise quantity of downstream leaves. Shoots were sampled in the tree canopy by professional climbers. Shoots were treated in the laboratory on the day they were sampled. For logistic reasons, two field sampling sessions were needed. The first one was dedicated to anatomical and vascular sampling, the second to mechanical sampling.

Anatomical traits

The first sampling session (January-July 2017) was dedicated to anatomical sampling. A total of 94 trees belonging to 42 species were sampled. Three trees per species were sampled in 20 species, two trees per species in 12 species, and one tree per species in the remaining 10 species (Table S1). In the laboratory, the leaves were cut off the stem of each shoot. The lengths of the stem and of the median leaf on the shoot were measured with a ruler to obtain the maximum conductive path length (L_{path}; cm). For compound-leaf species, the length of the rachis of the median leaf and the length of the leaflet of the median leaflet was added to obtain L_{path}. Total shoot leaf area (A_{leaf}; cm^2) was measured by scanning leaves and using ImageJ software (Table 1). We also measured the individual leaf area (cm^2) of the median leaf on each shoot to identify the range of leaf area across shoots and species (Table S1). The advantage of choosing the median leaf is that it is fully developed but not yet senescent.

A 1-cm-long stem section was sampled at the base of the shoot, from the internode supporting the last, oldest leaf. The sample was conserved in 50% ethanol. Anatomical cross-sections were made taking care to keep the section complete, and to avoid damaging any tissues. Anatomical sections were coloured with FASGA stain (safranin + Alcian blue). Images of each cross-section were digitised using an optical microscope (Olympus BX60; Olympus Corporation; Tokyo; Japan) at x50 magnification and a Canon EOS 500D (lens Olympus U-TVI-X; F 0.0; ISO 100; speed 1/25) camera. To obtain a complete picture of the cross-section, the images were assembled in a panorama using Kolor AutoPano Giga software (v.3.6). The digitised cross-sections were processed with CS5 Photoshop software (v.12.0). In addition to the complete cross-section, we considered four types of tissue: pith, xylem (primary and secondary xylems pooled together; A_{xylem}), phloem, and cortex. We manually delineated the tissues on the photographs (Fig. 1) and created masks. The masks for each layer were used to calculate the cross-sectional area (mm²) and fraction of each tissue, as well as the whole stem area using ImageJ software (v.1.43u).

Xylem vessels were analysed with ImageJ software to calculate theoretical xylem hydraulic properties (Abramoff *et al.*, 2003). For each vessel, we calculated the cross-sectional area (µm²) and elliptical diameters. To study variations in vessel dimensions, we used the mean hydraulic diameter (D_h, µm; see Table 1 for formula), i.e. the diameter that all vessels, considered as circles, would need to sustain the same tissue hydraulic conductivity (Tyree and Zimmermann, 2002). The total number of vessels was counted, enabling calculation of vessel density (VD; mm^{-2}). The cumulated vessel area (mm²) was considered as the sum of the cross-sectional area of all vessels (Table 1).

Following past studies (Anfodillo *et al.*, 2006; Olson *et al.*, 2014; Levionnois *et al.*, 2020), we estimated an overall widening rate across shoots (D_h/conductive path length) based on a slope of the log-log relationship between D_h at the base of the shoot, and the conductive path length, across all measured shoots.

Mechanical traits

The second field session (May-June 2018) was dedicated to quantifying mechanical traits on new shoots. A total of 50 trees belonging to 26 out of the 42 species sampled in the first field session were sampled again. Three trees per species were sampled in seven species, two trees per species in 11 species, and one tree per species in the remaining eight species. In the laboratory, the leaves were cut from the stem of each shoot. The modulus of elasticity was measured on the fresh stem on the day of sampling. The leaves were dried in an oven at 70 °C for 72 h. The leaf dry mass was measured with a precision scale and LMA (g m^{-2}) was quantified as the ratio of leaf dry mass to leaf area.

Before cutting the shoot at the internode supporting the last oldest leaf, but after removing all the leaves, the flexural stiffness (*EI*, kN mm²; Table 1) of the stem was measured based on a four-point bending method (Chapotin *et al.*, 2006). We measured the EI that is representative of the part of the stem that supports the leaves. The four-point bending method yields a mean value of *EI* along the axis. The stem was laid on two external supports, such that the length L between the external supports was 120 mm or 180 mm depending on the size of the shoot. The stem was laid such that the stem segment on the apex side was not deformed. The force was applied with an internal support, such that two points were in contact with the stem, and such that the length *L* between the two internal points was *L*/3 and the distance between an external point and the closest internal point was also *L*/3. To apply the force on the internal support, a basket was attached to it, and 10 g weights were successively added to the basket. The cross section equidistant from the two external supporting points was measured to obtain two orthogonal diameters. Stem tapering was previously shown to be negligible to calculate the flexural stiffness, based on stems of Guianese tropical tree species (Alméras *et al.*, 2009). A series of photos was taken successively with each additional 10 g load. The successive load was low to ensure small stem vertical deflection in comparison to the distance *L* between the two external supports, and such that it remained within the elastic behaviour domain. The successive vertical deflection length was measured for each additional 10-g load, relying on image analysis of each successive photo using ImageJ software. *EI* was calculated from the slope of this relationship (see Table 1 for the formula).

The second moment of area (I, mm^4) was calculated from the mean diameter of the cross section of the stem sample in the middle of the stem section between the supporting points of the bending apparatus (see Table 1 for the formula). *I* quantifies the distribution of material in a cross section with respect to the centre of the mass of the cross-section and describes the mechanical effect of cross-section geometry. The modulus of elasticity (MOE, kN mm^{-2}; Table 1) of the stem was calculated as *EI* divided by *I*.

Statistical analysis

We chose to sample a diverse range of species to cover the widest range of leaf and shoot size possible. Based on the number of individuals, some species in our dataset are poorly replicated. However, we assume this is not an issue as our aim was to study general scaling patterns across species. Therefore, all analyses were individual-based, not species-based. We think this is more appropriate for an allometric approach, as we wanted to link a precise conductive path length with a precise D_h, for instance, and as species-based means may affect precision. Likewise, the purpose of our study was to investigate the shoot level and to compare large and small leaves, not to compare "large-leaved" species with "small-leaved" species.

To model the scaling of the hydraulic constraint, i.e., the difference in water potential, we calculated the integrated trait $\Delta\Psi$ as:

$$\Delta\Psi = \frac{A_{leaf} \times L_{path}}{VD \times {D_h}^4 \times A_{xylem}}$$

To model the sizing of the mechanical constraint, i.e., the bending angle, we calculated the integrated trait ΔΦ as:

$$\Delta\Phi = \frac{LMA \times A_{leaf} \times {L_{stem}}^2}{MOE \times I}$$

R software (http://CRAN-R-project.org) was used for all statistical analyses. After log transformation, relationships between each trait Y and the shoot stem diameter D_{stem} were described as: $Y = a\ D_{stem}{}^{b}$, so that: $\log(Y) = \log(a) + b * \log(D_{stem})$, where b is the slope (or scaling exponent) and a is the intercept (allometric coefficient). To model the scaling of the hydraulic constraint and the mechanical constraint with stem diameter, we used ordinary least squares regression (OLS) to conserve the additivity of all slopes. In other words, the slope of the integrated traits ΔΨ and ΔΦ is equal to the sum of the slope of each trait, weighted by their exponent. For additivity to be conserved, missing values had to be retrieved. The model was then applied to 77 trees for the hydraulic constraint, and to 38 trees for the mechanical constraint. For each trait, the slope is compared to the slope of the theoretical case of isometry based on the standard error.

Bivariate log-log relationships were also presented between morphological, anatomical, vascular, and mechanical traits in all the trees available. Here we used standardised major axis regression (SMA) (Warton *et al.*, 2006), providing the error on both the *x*-axis and *y*-axis (Harvey and Pagel, 1991), in the SMATR package (Falster *et al.*, 2006). However, we used OLS for the relationship between D_h and the conductive path length, and between D_h and stem diameter, as the explanatory variable is more explicit (Fajardo *et al.*, 2020*a*; Olson *et al.*, 2021). A 95% confidence interval around the slope was used for SMA.

RESULTS

Shoot leaf area A_{leaf} ranged from 43 to 9,876 cm², with two to 23 leaves per shoot (Table S1). Individual leaf area ranged from 10 to 2,145 cm² (Table S1). The $A_{leaf} \propto A_{stem}$ scaling was positively and hypo-allometric (Fig. 2; Table 3), with a slope of 0.84 (0.75 – 0.95).

Regarding the scaling of the hydraulic constraint (quantified as the difference in water potential ΔΨ) with stem diameter D_{stem} ($\Delta\Psi \propto D_{stem}$), the slope was zero, deviating from theoretical prediction under the assumption of isometry (Table 2), meaning that ΔΨ was decoupled from shoot size. The $A_{leaf} \propto D_{stem}$ scaling did not significantly deviate from theoretical isometry. The $L_{path} \propto D_{stem}$, the VD $\propto D_{stem}$ and the $A_{xylem} \propto D_{stem}$ scaling were hypo-allometric contrary to the predicted theoretical isometry, such that their large deviation determines the $\Delta\Psi \propto D_{stem}$ scaling.The $D_h \propto D_{stem}$ scaling was hyper-allometric contrary to the predicted theoretical isometry.

Regarding the scaling of the mechanical constraint (quantified as the bending angle $\Delta\Phi$) as a function of D_{stem} ($\Delta\Phi \propto D_{stem}$), the slope was negative, and deviated strongly from theoretical prediction under the assumption of isometry (Table 2), meaning that the mechanical constraint is relatively lower for large shoots. The $I \propto D_{stem}$ scaling did not deviate from theoretical isometry. The LMA $\propto D_{stem}$ scaling, the $A_{leaf} \propto D_{stem}$ scaling, the $L_{stem} \propto D_{stem}$ scaling, and the MOE $\propto D_{stem}$ scaling, were all hypo-allometric contrary to the predicted theoretical isometry. The large deviation of the $L_{stem} \propto D_{stem}$ scaling determines the $\Delta\Phi \propto D_{stem}$ scaling.

The $D_h \propto L_{path}$ scaling was positive and hypo-allometric with a slope of 0.45 ± 0.06 (Fig. 3a; Table 3), as was $D_h \propto D_{stem}$ and $D_h \propto A_{leaf}$ scaling (Table 3). The 'xylem area $\propto A_{leaf}$' scaling was positive and hypo-allometric with a slope of 0.86 (0.78 – 0.96; Fig. 3b; Table 3). The 'total number of vessels $\propto A_{leaf}$' scaling was positive and hypo-allometric with a slope of 0.54 (0.46 – 0.64; Fig. 3c; Table 3). The 'cumulated vessel area $\propto A_{leaf}$' scaling was positive and hypo-allometric with a slope of 0.83 (0.73 – 0.93; Fig. 3d; Table 3). The MOE $\propto D_{stem}$ scaling was negative with a slope of -2.00 (-2.42 - -1.65; Fig. 4a), as was the MOE $\propto A_{leaf}$ scaling (Table 3). The $EI \propto D_{stem}$ scaling was positive with a slope of 2.73 (2.35 – 3.17; Fig. 4b), as was the $EI \propto A_{leaf}$ scaling (Table 3). In summary, large shoots displayed disproportionately less xylem area and vessels, while vessels were larger at shoot base. Also, large shoots displayed lower MOE, but were not less stiff due to increased *I*. The 'pith area $\propto A_{stem}$' scaling was positive and hyper-allometric with a slope of 1.25 (1.16 – 1.34; Fig. 5a; Table 3). Xylem, phloem, and cortex areas were positively and isometrically related to stem area (Fig. 5b, c, d; Table 3). Pith and cortex areas were positively and isometrically related to shoot leaf area (Table 3). The 'phloem area $\propto A_{leaf}$' scaling was positive and hypo-allometric with a slope of 0.85 (0.73 – 0.99; Table 3).

Based on species' means, most of the relationships and slopes were conserved (Table S2; Fig. S1; Fig. S2; Fig. S3; Fig. S4). The slope was substantially different for two relationships. The '$A_{leaf} \propto A_{stem}$' and the 'xylem area $\propto A_{leaf}$' scaling were positive but isometric, with a slope of 0.90 (0.79 – 1.03) and 0.91 (0.81 – 1.04), respectively (Fig. S1; Fig. S4).

DISCUSSION

We examined how the estimated water potential difference $\Delta\Psi$ and bending angle $\Delta\Phi$ scaled with shoot size, as they are potential limitations to the achievement of large leaves if isometric scaling is assumed between morphological and anatomical traits and shoot size (Eq. 2 and 4). We found no scaling of either hydraulic or mechanical constraints with increasing shoot size, as indicated by stem diameter (D_{stem}). The estimated $\Delta\Psi$ was independent of shoot size (Table 2), indicating that the risk of embolism spreading (i.e. too large $\Delta\Psi$), or that insufficient water supply (i.e. too low $\Delta\Psi$) because of the cumulated effects of large shoots and long path lengths are in fact limited. The estimated $\Delta\Phi$ was negatively linked to shoot size, which rather indicates that large shoots are overbuilt against the increased risk of bending with increasing loading weight. Taken together, these findings suggest that hydraulics and flexural mechanics are not limiting factors in driving leaf size variation and selection, at least not at the shoot level. We also show that hydraulic and mechanical functions are not in conflict at the shoot level, as they involve different trait adjustments that are independent of one another.

Hydraulics are not a limitation

The fact that hydraulics are not limiting factors in driving leaf size variation is explained by different traits deviating from the expected isometric scaling with D_{stem} at the shoot level. We found adjustments to conductive path length (L_{path}), vessel density (VD), vessel hydraulic diameter (D_h) and xylem area (A_{xylem}), while shoot leaf area was the only trait that followed isometric scaling with D_{stem}, as theoretically predicted (Table 2). The hypo-allometric $A_{xylem} \propto D_{stem}$ scaling deviated only slightly from isometry, suggesting disproportionately less conductive area with increasing shoot size. This shows that the effective adjustments to minimise the water potential difference $\Delta\Psi$ arise with L_{path} and D_h. The hypo-allometric $L_{path} \propto D_{stem}$ scaling suggests that the increase in hydraulic resistance (with increasing shoot size) is mitigated, as hydraulic resistance is proportional to the conductive path length, according to the Hagen-Poiseuille law (Tyree and Zimmermann, 2002). Finally, D_h increased with D_{stem}, L_{path} and shoot leaf area, which is certainly a crucial adjustment for the conservation of water supply across shoot size. The increase in D_h explains why VD decreases with D_{stem}, as there is a trade-off between vessel size and vessel number, known as the packing rule (Sperry *et al.*, 2006; Zanne *et al.*, 2010).

The increase in D_h with L_{path}, also termed tip-to-base axial vessel widening, is a well-known pattern usually described along the stem (Petit *et al.*, 2008, 2010; Bettiati *et al.*, 2012;

Anfodillo *et al.*, 2013; Olson *et al.*, 2014). To mitigate hydrodynamic resistance, hydraulic optimality models (West *et al.*, 1999) predict a minimum widening rate of 0.2 (i.e. $D_h \propto L_{path}^{0.2}$). This widening rate is found across all plants and trees when considering the stem vascular architecture (Anfodillo *et al.*, 2006, 2013; Petit *et al.*, 2014; Olson *et al.*, 2014, 2021). We estimated a widening rate of 0.45 ± 0.06 across shoots, which is higher than the predicted rate. Nevertheless, our findings are consistent with the results of several other studies showing that the vessel widening rate is not constant along the total path length and tends to be higher toward the apex of trees (Anfodillo *et al.*, 2006; Petit *et al.*, 2010; Bettiati *et al.*, 2012). Moreover, the widening rate has been found to be two to three times higher in leaves (Coomes *et al.*, 2008; Lechthaler *et al.*, 2019; Levionnois *et al.*, 2020). This increasing widening rate toward the apex or in leaves is probably linked to intense vessel furcation within the crown, within branches, and within leaves (Bettiati *et al.*, 2012; Lechthaler *et al.*, 2019). The increasing widening rate could also be linked to hydraulic segmentation within the crown or at stem-leaf and stem-petiole interfaces, since the hydraulic segmentation hypothesis assumes higher hydraulic resistance (or lower conductance) in leaf xylem than that in stem xylem (Tyree and Ewers, 1991; Tyree and Zimmermann, 2002; Pivovaroff *et al.*, 2014), based on vessel constriction (Zimmermann, 1978; Salleo *et al.*, 1984; André *et al.*, 1999).

Mechanics are not a limitation

The fact that flexural mechanics are not limiting factors in driving leaf size variation is explained by different traits deviating from the expected isometric scaling with D_{stem} at the shoot level. We found adjustments to LMA, shoot leaf area (A_{leaf}), stem length (L_{stem}) and modulus of elasticity (MOE), while the second moment of area I was the only trait following isometric scaling with D_{stem}, as theoretically predicted (Table 2). However, the hypo-allometric $A_{leaf} \propto D_{stem}$ scaling is certainly idiosyncratic, due to the small sample size (n = 39) and large standard error around the slope for these models describing the mechanical constraint and was contradicted by our result obtained with larger sample size (Fig. 2). Furthermore, even when we kept the scaling exponent of the $A_{leaf} \propto D_{stem}$ scaling at 2, the scaling exponent of the $\Delta\Phi \propto D_{stem}$ scaling remained clearly negative. The effective adjustments ensuring mechanical stability certainly arise from adjustments to LMA and L_{stem} with increasing shoot size. Constant LMA across the shoot size range buffers the increase in weight loading with increasing shoot size.

We found that L_{stem} decreased with D_{stem}. Consequently, the shorter the stem, the lower the cantilevered-beam effect of the stem and the higher the rigidity of the whole stem. However, based on the large standard error around the slope, the negative $L_{stem} \propto D_{stem}$ scaling is suspicious. (1) It contradicts the well-documented leaf size-leaf number trade-off, since large leaves are predicted to be more widely spaced (Kleiman and Aarssen, 2007; Xiang *et al.*, 2009; Dombroskie, 2012; Yan *et al.*, 2013; Fan *et al.*, 2017). (2) When we considered the shoot dataset for hydraulic traits (n = 97, result not shown), we found no relationship between L_{stem} and D_{stem}. Moreover, data are scarce for the $L_{stem} \propto D_{stem}$ scaling at the shoot level. Sun *et al.* (2019) found a hypo-allometric $L_{stem} \propto D_{stem}$ scaling at the twig level, supporting disproportionately less cantilevered loading for large twigs. As the flexural angle $\Delta\Phi$ is a two-powered function of L_{stem}, L_{stem} is a strong determinant of $\Delta\Phi$, and the $L_{stem} \propto D_{stem}$ scaling is a central parameter of mechanical stability and deserves more investigation in the frame of the LS-SS spectrum.

The negative $\Delta\Phi \propto D_{stem}$ scaling suggests that large shoots are overbuilt against the risk of bending that arises with increasing loading weight. Here, we only focused on the static loading of leaves. However, depending on the species, shoots have to temporarily but frequently support inflorescence and fruits, and there is a positive relationship between shoot size on the one hand, and inflorescence and fruit size on the other (Corner, 1949; Midgley and Bond, 1989; Ackerly and Donoghue, 1998; Westoby *et al.*, 2002; Westoby and Wright, 2003; Duivenvoorden and Cuello, 2012; Leslie *et al.*, 2014). Leaves also have to support wind drag forces (Niklas, 1996, 1999), even though large leaves generally have diverse forms and shapes to reduce possible drag forces (Vogel, 2009; Nicotra *et al.*, 2011). Finally, we measured the overall stem MOE, as both xylem and bark contribute to stem bending mechanics (Rosell and Olson, 2014; Clair *et al.*, 2019; Lehnebach *et al.*, 2020). This is particularly the case of the shoot level, since secondary growth has not, or just, begun. Therefore, to better identify the factors that shape the LS-SS spectrum, the relative contribution of the different mechanical constraints that apply to shoots (e.g., leaf and fruit loading, wind drag force), as the relative contribution of xylem vs. bark in shoot mechanical stability need to be better taken into account in future research.

Is there a hydraulic-mechanic trade-off?

Our results support the hypothesis that water supply and mechanical stability are not in strong conflict at the shoot level, contrary to the idea of a hydraulic-mechanical trade-off (Fan *et al.*, 2017). Only one trait seems to be involved in the two functions: the length of the stem or the whole conductive path. Indeed, minimising stem length makes it possible to minimise both hydraulic resistance and cantilevered loading. Minimising stem length also allows the minimising of carbon construction costs, but probably comes at the expense of light foraging (Olson *et al.*, 2018). Our results also support the hypothesis that the water supply is mainly maintained by axial vessel widening (i.e., allometric scaling of D_h with stem diameter and length), and that mechanical stability is rather determined by MOE and I. Our study also suggests that these traits (D_h, MOE, I) can vary relatively independently across the LS-SS spectrum while ensuring water supply and mechanical stability across the LS-SS spectrum.

We showed that xylem area was isometrically related to the section area, and allometrically related to shoot leaf area with disproportionately less xylem area for a larger shoot leaf area. Therefore, the increase in D_h does not require disproportionately more xylem area to supply water to large shoots. According to the Hagen-Poiseuille law, vessel conductivity scales at the fourth-power function of vessel diameter. Consequently, the increase in D_h increases xylem conductive efficiency, finally allowing for disproportionately fewer vessels and less cumulated vessel area per shoot leaf area with increasing stem diameter (Table 3). The hypo-allometric 'cumulated vessel area $\propto A_{leaf}$' scaling contradicts a recent finding in the leaf xylem of an *Acer* species (Lechthaler *et al.*, 2019), but may be explained by more intense vessel furcation across leaf veins. The increasing xylem conductive efficiency also allows for disproportionately less xylem area per shoot leaf area. The hyper-allometric $A_{leaf} \propto A_{xylem}$ scaling may be an anatomical explanation for the positive hyper-allometric scaling of $A_{leaf} \propto A_{stem}$ we found, and that is -to our knowledge- based on the widest range of individual leaf area sampled in a case study. However, when based on species' mean' (Table S2), $\mathrm{A_{leaf}} \propto \mathrm{A_{xylem}}$ and $\mathrm{A_{leaf}} \propto \mathrm{A_{stem}}$ scaling were isometric, despite trending towards allometry. Nevertheless, the conclusion remains the same as increasing xylem conductive efficiency allows to avoid disproportionately more xylem and stem cross-sectional areas –and subsequent construction costs- with increasing shoot size. The same explanation may apply to phloem, as we found positive hyper-allometric scaling for '$A_{leaf} \propto$ phloem area'. It has been shown that phloem sieve tubes also undergo tip-to-base axial widening, and to some extent obey the Hagen-Poiseuille law (Petit and Crivellaro, 2014).

The adjustment of shoot mechanical stability across the LS-SS spectrum does not imply adjustments to the xylem area. Rather, we observed hyper-allometric scaling of 'pith area $\propto A_{stem}$', leading to an increase in pith proportion with shoot size. As pith is mainly composed of large parenchyma cells with thin and poorly lignified cell walls (Evert, 2006), a higher pith fraction reduces the cost in biomass relative to stem volume in large stems. In turn, the increase in the pith fraction determines the decrease in stem density and MOE, but maximises *I* at low carbon cost. In a recent study (Olson *et al.*, 2018), this phenomenon was explained by assuming similar amounts of carbon to allocate across the existing range of stem sizes. As large leaves require greater spacing and a larger stem, and larger petiole and/or rachis volumes to support them, tissue density is consequently lower, in agreement with a volume-density trade-off, potentially driving the trade-off between MOE and *EI*. However, despite increasing *EI* with shoot size, our results indicate hypo-allometric $EI \propto D_{\mathrm{stem}}$ scaling, and consequently a reduction in the efficiency of *EI* with increasing shoot size. In this case, compensation may also arise with the minimisation of L_{stem} and LMA, as discussed above. In conclusion, mechanical stability is not a limitation for large shoots, but comes at the cost of L_{stem} if we assume it is linked to light foraging, as carbon limitation impedes the simultaneous maximisation of both mechanical stability and L_{stem}.

Future outlook

The fact that hydraulics and flexural mechanics are not limiting factors in driving leaf size variation at the shoot level is an important finding, as the evolutionary and ecological drivers of leaf size variation have not yet been fully disentangled (Westoby *et al.*, 2002; Yang *et al.*, 2010; Wright *et al.*, 2017). This is also the case of the identification of the selective value of large vs. small leaves within or across environments. The hypotheses explaining the coexistence of species with very contrasting leaf sizes at a local scale in rainforests remain weak. In our opinion, the differential selective value of leaf size has been explained by three different mechanisms. First, large leaves could be disadvantaged because of their sensitivity to heat which may cause an impairment of the photosynthetic apparatus (Leigh *et al.*, 2017). Larger leaves generally have thicker boundary layers, resulting in slower conductive heat loss. Second, leaf size has been hypothesised to play a role in the carbon cost-benefit balance of leaves and twigs. This has been investigated in particular in the frame of the ‘diminishing return’ hypothesis, and several studies support the hypothesis that larger leaves have a higher LMA, and that large leaves and twigs have disproportionately more dry mass than small ones (Niklas *et al.*, 2007, 2009; Niinemets *et al.*, 2007; Milla and Reich, 2007; Niklas and Cobb, 2008; Yang *et al.*, 2010). Based on a model, Yang *et al.* (2010) showed that large leaves and twigs should have a longer lifespan and/or higher photosynthetic assimilation rates, thereby counterbalancing the diminishing return. However, constraints related to heat dissipation and the diminishing return hypothesis do not explain why having large leaves could be advantageous. Third, leaf size can affect light interception efficiency (e.g. total absorbed photosynthetically active radiation per total leaf area) and self-shading, with large leaves maximising light interception efficiency and minimising self-shading (Duursma *et al.*, 2012; Smith *et al.*, 2014, 2017). Future investigations will require the quantification of carbon costs-benefits and light interception performances to better understand the selective pressure acting on large vs. small leaves and to better predict their ecological distribution.

The hyper-allometric $A_{\mathrm{leaf}} \propto A_{\mathrm{stem}}$ scaling in this study is in agreement with a majority of studies that investigated 'leaf area ∝ stem area' scaling, and supports hyper-allometry at the interspecific level (Brouat and McKey, 2001; Westoby and Wright, 2003; Preston and Ackerly, 2003; Sun *et al.*, 2006; Normand *et al.*, 2008; Xiang *et al.*, 2009; Yang *et al.*, 2009; Liu *et al.*, 2010; Yan *et al.*, 2013; Osada *et al.*, 2015). Our study contradicts two studies that support isometry (Brouat *et al.*, 1998; Fan *et al.*, 2017). Nevertheless, across these studies, the slope of the 'leaf area ∝ stem area' scaling ranges from 1.0 to 1.8, suggesting it is context-dependant and sensitive to parameters such as the size of the sample, the range of leaf sizes, the largest leaf area in the sample, and the biome (e.g., temperate vs. tropical) concerned. Analysing data at the individual or species' level can also affect statistical results, as our $\mathrm{A}_{\mathrm{leaf}} \propto \mathrm{A}_{\mathrm{stem}}$ and $\mathrm{A}_{\mathrm{leaf}} \propto \mathrm{A}_{\mathrm{sylem}}$ scaling turned isometric based on species' means (Table S2). However, this may be statistically induced by the de facto reduction in the sample size and the magnitude of trait variation. Moreover, when investigated at the intraspecific level, the slope of the 'leaf area ∝ stem area' scaling has been shown to be species dependant, with some species exhibiting isometric, hypo-allometric, and hyper-allometric scaling (Brouat *et al.*, 1998; Brouat and McKey, 2001; Preston and Ackerly, 2003; Normand *et al.*, 2008; Yan *et al.*, 2013; Fajardo *et al.*, 2020*b*). Therefore, further investigations are required to dedicatedly identify the trending slope of the 'leaf area ∝ stem area' scaling at global level, which would certainly benefit from a meta-analysis incorporating the widest range of leaf area across biomes. One way forward would also be to dedicatedly investigate the diversity of intraspecific scaling, as the scaling exponent can be considered as a trait in its own right, with its own adaptive value (Preston and Ackerly, 2003; Vasseur *et al.*, 2012, 2018).

DATA AVAILABILITY STATEMENT

The data supporting the findings of this study are available from the corresponding authors, (S. Levionnois and P. Heuret), upon request.

ACKNOWLEDGEMENTS

Special thanks to Maryline Harroué and Julien Ruelle from the SILVATECH facility (UMR SILVA) for performing significant part of the anatomical cuts. We thank the climbing team for canopy sampling: Jocelyn Cazal, Valentine Alt, Samuel Counil, Anthony Percevaux, and Elodie Courtois. We thank all the field technical assistants: Oscar Affholder, Louise Authier, Benoit Burban, Elia Dardevet, Frederic Fung Fong You, Eva Gril, Ruth Tchana Wandji.

The author(s) would like to thank SILVATECH (Silvatech, INRA, 2018. Structural and functional analysis of tree and wood Facility, doi: 10.15454/1.5572400113627854E12) from UMR 1434 SILVA, 1136 IAM, 1138 BEF and 4370 EA LERMAB EEF research centre INRA Nancy-Lorraine for their contribution to the anatomical cuts. SILVATECH facility is supported by the French National Research Agency through the Laboratory of Excellence ARBRE (ANR-11-LABX-0002-01).

This study was funded by the GFclim project (FEDER 20142020, Project GY0006894) and an "*Investissement d'Avenir*" grant from the *Agence Nationale de la Recherche* (CEBA: ANR-10-LABX-0025; ARBRE, ANR-11-LABX-0002-01). S.L. was supported by a doctoral fellowship from CEBA.

AUTHOR CONTRIBUTION

P.H. and S.L. conceived and designed the study; S.L, C.Z., S.C., Cl.S., P.H. and A.G.-M. collected field samples; S.L., Ca.S and C.H. performed anatomical sections; S.L., Ca.S and P.H. performed images analysis; S.L and A.G.-M. measured morphological traits; S.L. B.C. measured mechanical traits; S.L., Ca.S., P.H and T.A. performed data analysis; S.L., P.H., T.A. and B.C. wrote the manuscript; all the authors discussed the results and contributed valuable comments on the manuscript.

LITERATURE

Abramoff M, Magalhães P, Ram SJ. 2003. Image Processing with ImageJ. Biophotonics International **11**, 36–42.

Ackerly D, Donoghue MJ. 1998. Leaf size, sapling allometry, and Corner's rules: phylogeny and correlated evolution in maples (Acer). The American Naturalist **152**, 767–791.

Aguilos M, Stahl C, Burban B, Herault B, Courtois EA, Coste S, Wagner F, Ziegler C, Takagi K, Bonal D. 2019. Interannual and seasonal variations in ecosystem transpiration and water use efficiency in a tropical rainforest. Forests **10**, 20.

Alméras T, Derycke M, Jaouen G, Beauchêne J, Fournier M. 2009. Functional diversity in gravitropic reaction among tropical seedlings in relation to ecological and developmental traits. Journal of Experimental Botany **60**, 4397–4410.

André J, Catesson AM, Liberman M. 1999. Characters and origin of vessels with heterogenous structure in leaf and flower abscission zones. Canadian Journal of Botany **77**, 253–261.

Anfodillo T, Carraro V, Carrer M, Fior C, Rossi S. 2006. Convergent tapering of xylem conduits in different woody species. New Phytologist **169**, 279–290.

Anfodillo T, Petit G, Crivellaro A. 2013. Axial conduit widening in woody species: a still neglected anatomical pattern. IAWA Journal **34**, 352–364.

Baas P, Ewers FW, Davis SD, Wheeler EA. 2004. 15 - Evolution of xylem physiology. In: Hemsley AR,, In: Poole I, eds. The Evolution of Plant Physiology. Oxford: Academic Press, 273–295.

Bettiati D, Petit G, Anfodillo T. 2012. Testing the equi-resistance principle of the xylem transport system in a small ash tree: empirical support from anatomical analyses. Tree Physiology **32**, 171–177.

Bittencourt PRL, Pereira L, Oliveira RS. 2016. On xylem hydraulic efficiencies, wood space-use and the safety–efficiency tradeoff. New Phytologist **211**, 1152–1155.

Brouat C, Gibernau M, Amsellem L, McKey D. 1998. Corner's Rules revisited: ontogenetic and interspecific patterns in leaf-stem allometry. The New Phytologist **139**, 459–470.

Brouat C, McKey D. 2001. Leaf- stem allometry, hollow stems, and the evolution of caulinary domatia in myrmecophytes. New Phytologist **151**, 391–406.

Chapotin SM, Razanameharizaka JH, Holbrook NM. 2006. A biomechanical perspective on the role of large stem volume and high water content in baobab trees (Adansonia spp.; Bombacaceae). American Journal of Botany **93**, 1251–1264.

Chave J, Coomes D, Jansen S, Lewis SL, Swenson NG, Zanne AE. 2009. Towards a worldwide wood economics spectrum. Ecology Letters **12**, 351–366.

Clair B, Ghislain B, Prunier J, Lehnebach R, Beauchêne J, Alméras T. 2019. Mechanical contribution of secondary phloem to postural control in trees: the bark side of the force. New Phytologist **221**, 209–217.

Coomes DA, Heathcote S, Godfrey ER, Shepherd JJ, Sack L. 2008. Scaling of xylem vessels and veins within the leaves of oak species., Scaling of xylem vessels and veins within the leaves of oak species. Biology letters, Biology Letters **4, 4**, 302, 302–306.

Corner EJH. 1949. The Durian Theory or the origin of the modern tree. Annals of Botany **13**, 367–414.

Cruiziat P, Cochard H, Améglio T. 2002. Hydraulic architecture of trees: main concepts and results. Annals of Forest Science **59**, 723–752.

Dombroskie S. 2012. The leaf size/number trade-off within species and within plants for woody angiosperms. Plant Ecology and Evolution **145**, 38–45.

Duivenvoorden JF, Cuello NL. 2012. Functional trait state diversity of Andean forests in Venezuela changes with altitude. Journal of Vegetation Science **23**, 1105–1113.

Duursma RA, Falster DS, Valladares F, *et al.* 2012. Light interception efficiency explained by two simple variables: a test using a diversity of small- to medium-sized woody plants. New Phytologist **193**, 397–408.

Evert R. 2006. Parenchyma and collenchyma. Esau's Plant Anatomy. Wiley-Blackwell, 175–190.

Fajardo A, Martínez- Pérez C, Cervantes- Alcayde MA, Olson ME. 2020*a*. Stem length, not climate, controls vessel diameter in two trees species across a sharp precipitation gradient. New Phytologist **225**, 2347–2355.

Fajardo A, Mora JP, Robert E. 2020*b*. Corner's rules pass the test of time: little effect of phenology on leaf–shoot and other scaling relationships. Annals of Botany **126**, 1129–1139.

Falster DS, Warton DI, Wright II. 2006. User's guide to SMATR: Standardised Major Axis Tests & Routines Version 2.0, Copyright 2006. R instructions.

Fan Z-X, Sterck F, Zhang S-B, Fu P-L, Hao G-Y. 2017. Tradeoff between stem hydraulic efficiency and mechanical strength affects leaf-stem allometry in 28 Ficus tree species. Frontiers in Plant Science **8**, 1619.

Gourlet-Fleury S, Guehl JM, Laroussine O. 2004. *Ecology and management of a neotropical rainforest : lessons drawn from Paracou, a long-term experimental research site in French Guiana*. Paris: Elsevier.

Hallé F, Oldeman RAA, Tomlinson PB. 1978. *Tropical trees and forests - An architectural analysis*. Springer-Verlag Berlin Heidelberg.

Harvey PH, Pagel MD. 1991. *The comparative method in evolutionary biology*. Oxford University Press.

Kleiman D, Aarssen LW. 2007. The leaf size/number trade-off in trees. Journal of Ecology **95**, 376–382.

Lachenbruch B, McCulloh KA. 2014. Traits, properties, and performance: how woody plants combine hydraulic and mechanical functions in a cell, tissue, or whole plant. The New Phytologist **204**, 747–764.

Lauri P-É. 2019. Corner's rules as a framework for plant morphology, architecture and functioning – issues and steps forward. New Phytologist **221**, 1679–1684.

Lechthaler S, Colangeli P, Gazzabin M, Anfodillo T. 2019. Axial anatomy of the leaf midrib provides new insights into the hydraulic architecture and cavitation patterns of Acer pseudoplatanus leaves. Journal of Experimental Botany **70**, 6195–6201.

Lehnebach R, Alméras T, Clair B. 2020. How does bark contribution to postural control change during tree ontogeny? A study of six Amazonian tree species. Journal of Experimental Botany **71**, 2641–2649.

Leigh A, Sevanto S, Close JD, Nicotra AB. 2017. The influence of leaf size and shape on leaf thermal dynamics: does theory hold up under natural conditions? Plant, Cell & Environment **40**, 237–248.

Leslie AB, Beaulieu JM, Crane PR, Donoghue MJ. 2014. Cone size is related to branching architecture in conifers. New Phytologist **203**, 1119–1127.

Levionnois S, Coste S, Nicolini E, Stahl C, Morel H, Heuret P. 2020. Scaling of petiole anatomies, mechanics and vasculatures with leaf size in the widespread Neotropical pioneer tree species Cecropia obtusa Trécul (Urticaceae). Tree Physiology **40**, 245–258.

Liu Z, Cai Y, Li K, Guo J. 2010. The leaf size-twig size spectrum in evergreen broadleaved forest of subtropical China. African Journal of Biotechnology **9**, 3382–3387.

Martin- StPaul N, Delzon S, Cochard H. 2017. Plant resistance to drought depends on timely stomatal closure. Ecology Letters **20**, 1437–1447.

Midgley J, Bond W. 1989. Leaf size and inflorescence size may be allometrically related traits. Oecologia **78**, 427–429.

Milla R, Reich PB. 2007. The scaling of leaf area and mass: the cost of light interception increases with leaf size. Proceedings of the Royal Society B: Biological Sciences **274**, 2109–2115.

Nicotra AB, Leigh A, Boyce CK, Jones CS, Niklas KJ, Royer DL, Tsukaya H. 2011. The evolution and functional significance of leaf shape in the angiosperms. Functional Plant Biology **38**, 535–552.

Niinemets U, Portsmuth A, Tena D, Tobias M, Matesanz S, Valladares F. 2007. Do we underestimate the importance of leaf size in plant economics? Disproportional scaling of support costs within the spectrum of leaf physiognomy. Annals of Botany **100**, 283–303.

Niklas KJ. 1996. Differences between Acer saccharum Leaves from Open and Wind-Protected Sites. Annals of Botany **78**, 61–66.

Niklas KJ. 1999. A mechanical perspective on foliage leaf form and function. New Phytologist **143**, 19–31.

Niklas KJ, Cobb ED. 2008. Evidence for "diminishing returns" from the scaling of stem diameter and specific leaf area. American Journal of Botany **95**, 549–557.

Niklas KJ, Cobb ED, Niinemets Ü, Reich PB, Sellin A, Shipley B, Wright IJ. 2007. "Diminishing returns" in the scaling of functional leaf traits across and within species groups. Proceedings of the National Academy of Sciences **104**, 8891–8896.

Niklas KJ, Cobb ED, Spatz H-C. 2009. Predicting the allometry of leaf surface area and dry mass. American Journal of Botany **96**, 531–536.

Normand F, Bissery C, Damour G, Lauri P-É. 2008. Hydraulic and mechanical stem properties affect leaf–stem allometry in mango cultivars. New Phytologist **178**, 590–602.

Olson ME, Anfodillo T, Gleason SM, McCulloh KA. 2021. Tip-to-base xylem conduit widening as an adaptation: causes, consequences, and empirical priorities. New Phytologist **229**, 1877–1893.

Olson ME, Anfodillo T, Rosell JA, Petit G, Crivellaro A, Isnard S, León-Gómez C, Alvarado-Cárdenas LO, Castorena M. 2014. Universal hydraulics of the flowering plants: vessel diameter scales with stem length across angiosperm lineages, habits and climates. Ecology Letters **17**, 988–997.

Olson ME, Rosell JA, Zamora Muñoz S, Castorena M. 2018. Carbon limitation, stem growth rate and the biomechanical cause of Corner's rules. Annals of Botany **122**, 583–592.

Osada N, Nabeshima E, Hiura T. 2015. Geographic variation in shoot traits and branching intensity in relation to leaf size in Fagus crenata: A common garden experiment. American Journal of Botany.

Petit G, Anfodillo T, Mencuccini M. 2008. Tapering of xylem conduits and hydraulic limitations in sycamore (Acer pseudoplatanus) trees. New Phytologist **177**, 653–664.

Petit G, Crivellaro A. 2014. Comparative axial widening of phloem and xylem conduits in small woody plants. Trees **28**, 915–921.

Petit G, DeClerck FAJ, Carrer M, Anfodillo T. 2014. Axial vessel widening in arborescent monocots. Tree Physiology **34**, 137–145.

Petit G, Pfautsch S, Anfodillo T, Adams MA. 2010. The challenge of tree height in Eucalyptus regnans: when xylem tapering overcomes hydraulic resistance. The New Phytologist **187**, 1146–1153.

Pivovaroff A, Sack S, Santiago L. 2014. Coordination of stem and leaf hydraulic conductance in southern California shrubs: a test of the hydraulic segmentation hypothesis. New Phytologist **203**, 842–850.

Preston KA, Ackerly DD. 2003. Hydraulic architecture and the evolution of shoot allometry in contrasting climates. American Journal of Botany **90**, 1502–1512.

Rosell JA, Olson ME. 2014. The evolution of bark mechanics and storage across habitats in a clade of tropical trees. American Journal of Botany **101**, 764–777.

Salleo S, Gullo M a. L, Siracusano L. 1984. Distribution of vessel ends in stems of some diffuse- and ring-porous trees: the nodal regions as 'safety zones' of the water conducting system. Annals of Botany **54**, 543–552.

Shingleton A. 2010. Allometry: the study of biological scaling. Nature Education **3**, 2.

Smith DD, Sperry JS, Adler FR. 2017. Convergence in leaf size versus twig leaf area scaling: do plants optimize leaf area partitioning? Annals of Botany **119**, 447–456.

Smith DD, Sperry JS, Enquist BJ, Savage VM, McCulloh KA, Bentley LP. 2014. Deviation from symmetrically self-similar branching in trees predicts altered hydraulics, mechanics, light interception and metabolic scaling. New Phytologist **201**, 217–229.

Sperry JS, Adler FR, Campbell GS, Comstock JP. 1998. Limitation of plant water use by rhizosphere and xylem conductance: results from a model. Plant, Cell & Environment **21**, 347–359.

Sperry JS, Hacke UG, Pittermann J. 2006. Size and function in conifer tracheids and angiosperm vessels. American Journal of Botany **93**, 1490–1500.

Sun S, Jin D, Shi P. 2006. The leaf size–twig size spectrum of temperate woody species along an altitudinal gradient: an invariant allometric scaling relationship. Annals of Botany **97**, 97–107.

Sun J, Wang M, Lyu M, Niklas KJ, Zhong Q, Li M, Cheng D. 2019. Stem diameter (and not length) limits twig leaf biomass. Frontiers in Plant Science **10**.

Tyree MT, Ewers FW. 1991. The hydraulic architecture of trees and other woody plants. New Phytologist **119**, 345–360.

Tyree MT, Sperry JS. 1989. Vulnerability of xylem to cavitation and embolism. Annual Review of Plant Physiology and Plant Molecular Biology **40**, 19–36.

Tyree MT, Zimmermann MH. 2002. *Xylem Structure and the Ascent of Sap*. Berlin Heidelberg: Springer-Verlag.

Vasseur F, Exposito-Alonso M, Ayala-Garay OJ, Wang G, Enquist BJ, Vile D, Violle C, Weigel D. 2018. Adaptive diversification of growth allometry in the plant Arabidopsis thaliana. Proceedings of the National Academy of Sciences **115**, 3416–3421.

Vasseur F, Violle C, Enquist BJ, Granier C, Vile D. 2012. A common genetic basis to the origin of the leaf economics spectrum and metabolic scaling allometry. Ecology Letters **15**, 1149–1157.

Vogel S. 2009. Leaves in the lowest and highest winds: temperature, force and shape. New Phytologist **183**, 13–26.

Warton DI, Wright IJ, Falster DS, Westoby M. 2006. Bivariate line- fitting methods for allometry. Biological Reviews **81**, 259–291.

West GB, Brown JH, Enquist BJ. 1999. A general model for the structure and allometry of plant vascular systems. Nature **400**, 664–667.

Westoby M, Falster DS, Moles AT, Vesk PA, Wright IJ. 2002. Plant ecological strategies: some leading dimensions of variation between species. Annual Review of Ecology and Systematics **33**, 125–159.

Westoby M, Wright IJ. 2003. The leaf size – twig size spectrum and its relationship to other important spectra of variation among species. Oecologia **135**, 621–628.

White PS. 1983*a*. Corner's Rules in Eastern deciduous trees: allometry and its implications for the adaptive architecture of trees. Bulletin of the Torrey Botanical Club **110**, 203–212.

White PS. 1983*b*. Evidance that temperate east north american evergreen woody plants follow Corner's rule. New Phytologist **95**, 139–145.

Whitehead D, Edwards WRN, Jarvis PG. 1984. Conducting sapwood area, foliage area, and permeability in mature trees of Picea sitchensis and Pinus contorta. Canadian journal of forest research = Journal canadienne de la recherche forestiere.

Wright IJ, Dong N, Maire V, *et al.* 2017. Global climatic drivers of leaf size. Science **357**, 917–921.

Xiang S, Liu Y, Fang F, Wu N, Sun S. 2009. Stem architectural effect on leaf size, leaf number, and leaf mass fraction in plant twigs of woody species. International Journal of Plant Sciences **170**, 999–1008.

Yan E-R, Wang X-H, Chang SX, He F. 2013. Scaling relationships among twig size, leaf size and leafing intensity in a successional series of subtropical forests. Tree Physiology **33**, 609–617.

Yang D, Li G, Sun S. 2009. The effects of leaf size, leaf habit, and leaf form on leaf/stem relationships in plant twigs of temperate woody species. Journal of Vegetation Science **20**, 359–366.

Yang D, Niklas KJ, Xiang S, Sun S. 2010. Size-dependent leaf area ratio in plant twigs: implication for leaf size optimization. Annals of Botany **105**, 71–77.

Zanne AE, Westoby M, Falster DS, Ackerly DD, Loarie SR, Arnold SEJ, Coomes DA. 2010. Angiosperm wood structure: Global patterns in vessel anatomy and their relation to wood density and potential conductivity. American Journal of Botany **97**, 207–215.

Zimmermann MH. 1978. Hydraulic architecture of some diffuse-porous trees. Canadian Journal of Botany **56**, 2286–2295.

TABLES

Table 1. List of measured traits, abbreviations, and formulae.

Trait	**Unit**	**Abbreviation**	**Formula**
Stem cross-sectional area	mm^2	A_{stem}	
Stem cross-sectional diameter	mm	D_{stem}	
Shoot leaf area	cm^2	A_{leaf}	
Leaf dry mass per leaf area	$g\ m^{-2}$	LMA	$LMA = \text{leaf dry mass}/A_{leaf}$
Pith, xylem, phloem, cortex cross-sectional areas	mm^2	A_{xylem}: xylem area	
Stem length studied for stem bending	cm	L_{stem}	
Flexural stiffness	$kN\ mm^2$	EI	$EI = b \times \frac{l_1^3}{48} \times \left(\frac{3 \times l_2}{l_1} - \left(4 \times \left(\frac{l_2}{l_1} \right)^3 \right) \right)$ with b the force-deformation slope ($kN\ mm^{-1}$) l_1 and l_2 distances (mm) between external supporting and internal pressing points respectively
Second moment of area	mm^4	I	$I = \pi D^4/64$ with D the stem cross-sectional diameter
Modulus of elasticity	$kN\ mm^{-2}$	MOE	$MOE = EI/I$
Conductive path length	cm	L_{path}	
Mean hydraulic diameter	µm	D_h	$D_h = (\Sigma D_v^4/N)^{1/4}$
Vessel hydraulic diameter	µm		$D_v = [32(ab)^3/(a^2+b^2)]^{1/4}$ a and b major and minor ellipse diameters
Number of vessels		N_{vessel}	
Cumulated vessel area	$µm^2$		$N_{vessel} * \pi(D_h/2)^2$
Vessel density	mm^{-2}	VD	$VD = N_{vessel}/A_{xylem}$

Table 2. Estimation of the hydraulic and mechanical constraints and scaling with shoot size D_{stem}.

Water supply				Flexural support			
Trait	**OLS (slope ± SE)**	**Expected slope for isometry**	**R^2**	**Trait**	**OLS (slope ± SE)**	**Expected slope for isometry**	**R^2**
A_{leaf}	1.982 ± 0.124***	2	0.776	LMA	0.055 ± 0.124^{NS}	1	0.005
L_{path}	0.585 ± 0.087***	1	0.378	A_{leaf}	1.203 ± 0.323***	2	0.278
VD	-0.980 ± 0.144***	0	0.381	L_{stem}	-0.703 ± 0.302*	1	0.131
D_h	0.414 ± 0.061***	0	0.381	MOE	-1.760 ± 0.176***	0	0.736
A_{xylem}	1.852 ± 0.101***	2	0.819	I	3.999 ± 0.023***	4	0.999
$\Delta\Psi$	0.034 ± 0.199^{NS}	1	0.000	$\Delta\Phi$	-2.388 ± 0.833**	1	0.186
$\Delta\Psi = A_{leaf} + L_{path} - VD - 4 \times D_h - A_{xylem}$				$\Delta\Phi = \mu + A_{leaf} + 2 \times L_{stem} - MOE - I$			

All relationships were tested at a log-log scale. The significance of the relationship was tested: ***: $P < 0.001$; **: $P < 0.01$; *: $P < 0.05$: NS: $P > 0.05$. Standard errors are shown.

Table 3. Log-log bivariate relationships.

Regression	***Y***	***X***	***P***	***R*²**	**slope**	**CI**
SMA	Stem area	Shoot leaf area	**< 0.001**	0.702	0.834	0.742 – 0.937
SMA	Pith area	Shoot leaf area	**< 0.001**	0.689	0.992	0.887 – 1.110
SMA	Xylem area	Shoot leaf area	**< 0.001**	0.770	0.863	0.776 – 0.961
SMA	Phloem area	Shoot leaf area	**< 0.001**	0.608	0.849	0.731 – 0.985
SMA	Cortex area	Shoot leaf area	**< 0.001**	0.467	0.864	0.745 – 1.002
SMA	Pith area	Stem area	**< 0.001**	0.883	1.249	1.163 – 1.341
SMA	Xylem area	Stem area	**< 0.001**	0.805	1.003	0.915 – 1.100
SMA	Phloem area	Stem area	**< 0.001**	0.861	1.015	0.932 – 1.106
SMA	Cortex area	Stem area	**< 0.001**	0.899	1.034	0.968 – 1.105
SMA	MOE	Stem diameter	**< 0.001**	0.611	-2.000	-2.424 - -1.650
SMA	EI	Stem diameter	**< 0.001**	0.800	2.733	2.354 – 3.173
SMA	MOE	Shoot leaf area	**< 0.01**	0.156	-0.823	-1.096 - -0.619
SMA	EI	Shoot leaf area	**< 0.001**	0.248	0.947	0.684 – 1.311
OLS	D_h	Hydraulic path length	**< 0.001**	0.407	0.447 ± 0.061	
SMA	Number of vessels	Hydraulic path length	**< 0.001**	0.216	1.322	1.057 – 1.652
SMA	Cum. vessel area	Hydraulic path length	**< 0.001**	0.533	1.934	1.627 – 2.300
OLS	D_h	Stem diameter	**< 0.001**	0.308	0.364 ± 0.057	
SMA	Number of vessels	Stem area	**< 0.001**	0.508	0.709	0.606 – 0.829
SMA	Cum. vessel area	Stem area	**< 0.001**	0.710	0.987	0.879 – 1.108
SMA	D_h	Shoot leaf area	**< 0.001**	0.324	0.268	0.222 – 0.323
SMA	Number of vessels	Shoot leaf area	**< 0.001**	0.475	0.542	0.458 – 0.640
SMA	Cum. vessel area	Shoot leaf area	**< 0.001**	0.715	0.825	0.729 – 0.934

Bold values refer to significant correlations ($P < 0.05$). See Table 1 for a list of abbreviations. For OLS, the standard error is shown.

FIGURE LEGENDS

Fig. 1. Typical leafy shoots with simple leaves (left) and compound leaves (right). A complete compound leaf is shown. In the context of our study, a shoot is defined as a single unbranched stem supporting the most leaves, with no leaves missing between the youngest and the oldest leaf. Shoots were selected to avoid damaged leaves. Anatomical cross-sections were made at the base of each shoot to measure tissue cross-sectional area and fractions, vascular architecture, and theoretical hydraulic conductivity.

Fig. 2. Stem cross-sectional area according to shoot leaf area at a log-log scale. b: scaling exponent and its 95% CI in square brackets. * $P < 0.05$; ** $P < 0.01$; *** $P < 0.001$.

Fig. 3. Scaling of vascular traits with conductive path length and shoot leaf area, respectively. (A) Mean vessel hydraulic diameter according to conductive path length. (B) Xylem area according to shoot leaf area. (C) The number of vessels according to shoot leaf area. (D) Cumulated vessel area according to shoot leaf area. All results are at log-log scale. b: scaling exponent and its CI in square brackets based on SMA, except for (A) where the standard error is shown based on OLS. * $P < 0.05$; ** $P < 0.01$; *** $P < 0.001$.

Fig. 4. Scaling of mechanical traits with the stem cross-sectional area. (A) Stem modulus of elasticity (MOE) according to the stem cross-sectional diameter. (B) Flexural stiffness (EI) according to the stem cross-sectional area. All results are at log-log scale. b: scaling exponent and its CI in square brackets based on SMA. * $P < 0.05$; ** $P < 0.01$; *** $P < 0.001$.

Fig. 5. Scaling of stem tissue cross-sectional area with shoot leaf area. (A) Pith cross-sectional area according to shoot leaf area. (B) Xylem cross-sectional area according to shoot leaf area. (C) Phloem cross-sectional area according to shoot leaf area. (D) Cortex cross-sectional area according to shoot leaf area. All results are at log-log scale. b: scaling exponent and its CI in square brackets based on SMA. * $P < 0.05$; ** $P < 0.01$; *** $P < 0.001$.

Figure 1

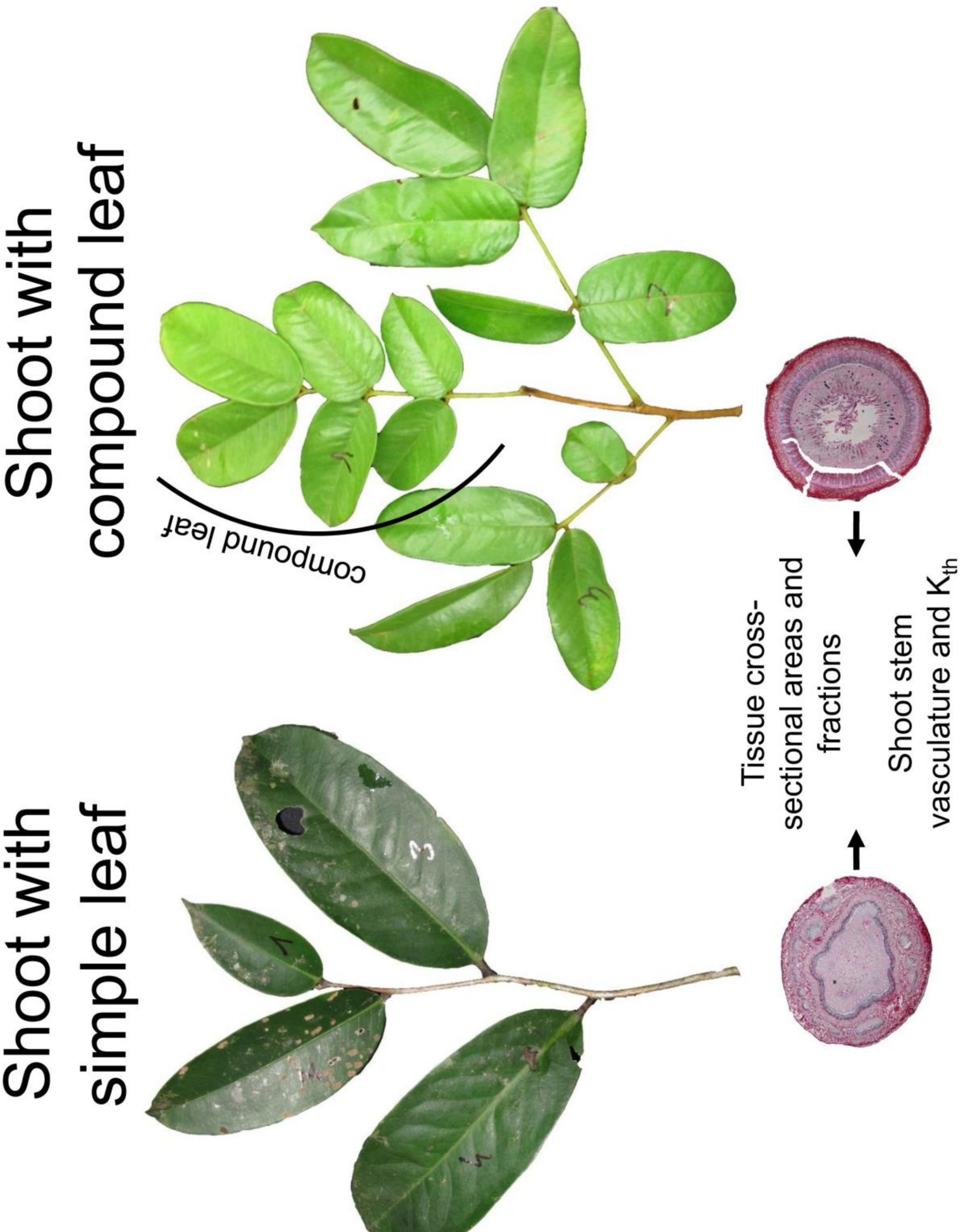

Shoot with simple leaf
Shoot with compound leaf
compound leaf
Tissue cross-sectional areas and fractions
Shoot stem vasculature and K_{th}

Figure 2

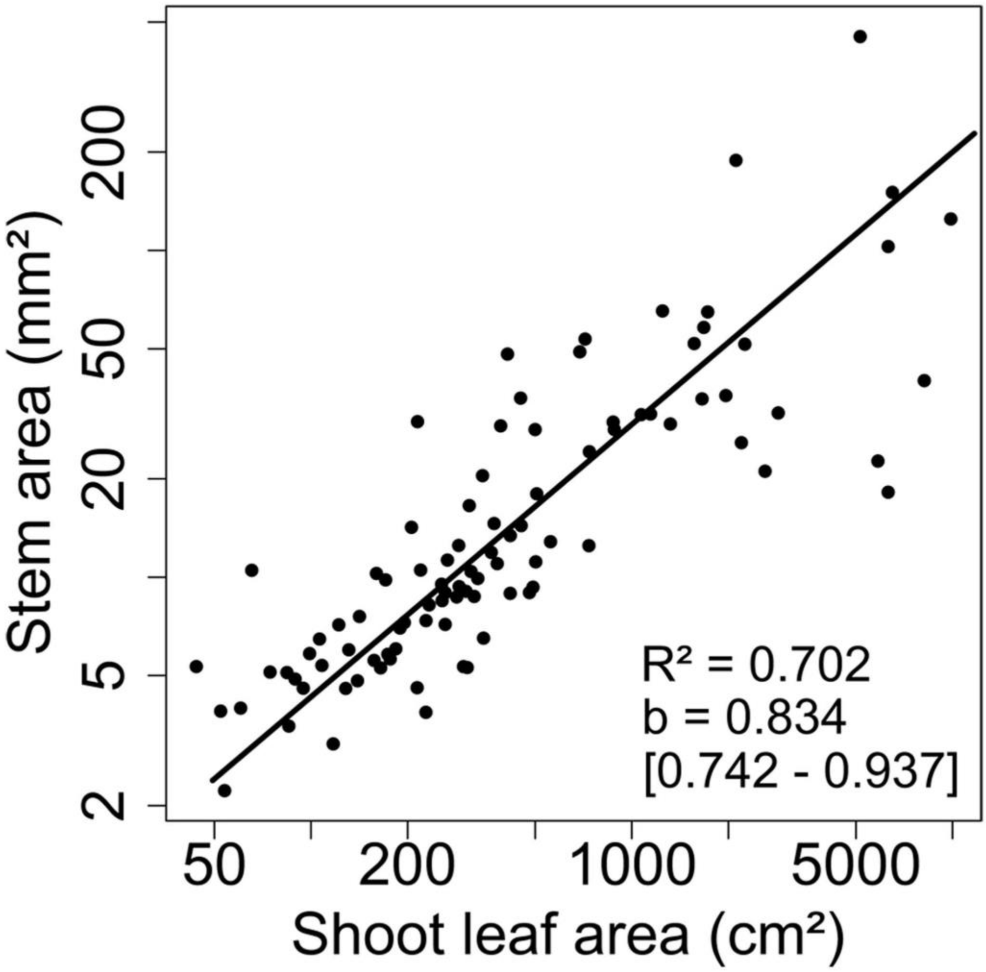

Stem area (mm²)
200
50
20
5
2
50
200
1000
5000
Shoot leaf area (cm²)
R² = 0.702
b = 0.834
[0.742 - 0.937]

Figure 3

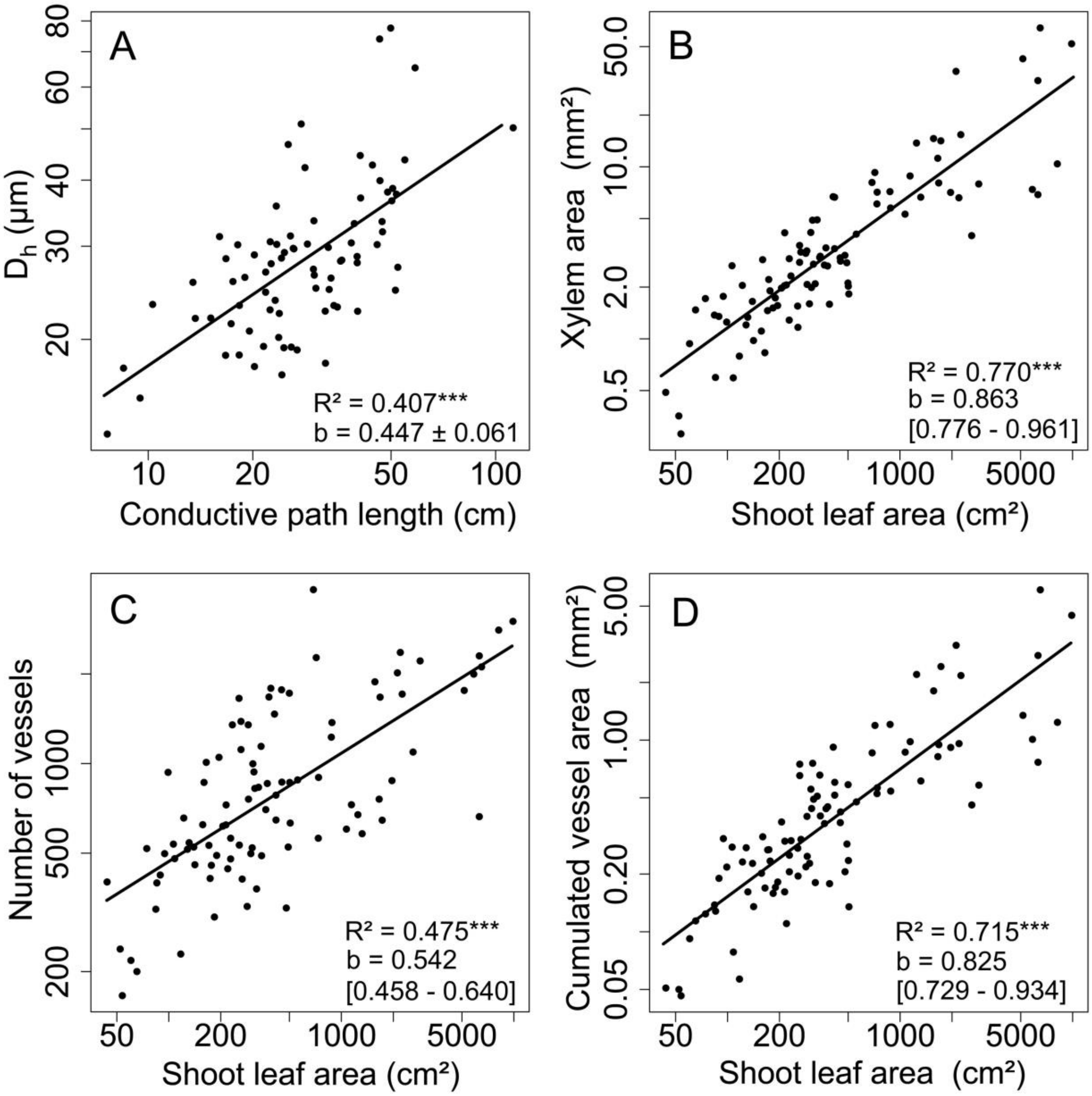

A
D_h (µm)
80
60
40
30
20
R² = 0.407***
b = 0.447 ± 0.061
10
20
50
100
Conductive path length (cm)
B
Xylem area (mm²)
50.0
10.0
2.0
0.5
R² = 0.770***
b = 0.863
[0.776 - 0.961]
50
200
1000
5000
Shoot leaf area (cm²)
C
Number of vessels
1000
500
200
R² = 0.475***
b = 0.542
[0.458 - 0.640]
50
200
1000
5000
Shoot leaf area (cm²)
D
Cumulated vessel area (mm²)
5.00
1.00
0.20
0.05
R² = 0.715***
b = 0.825
[0.729 - 0.934]
50
200
1000
5000
Shoot leaf area (cm²)

Figure 4

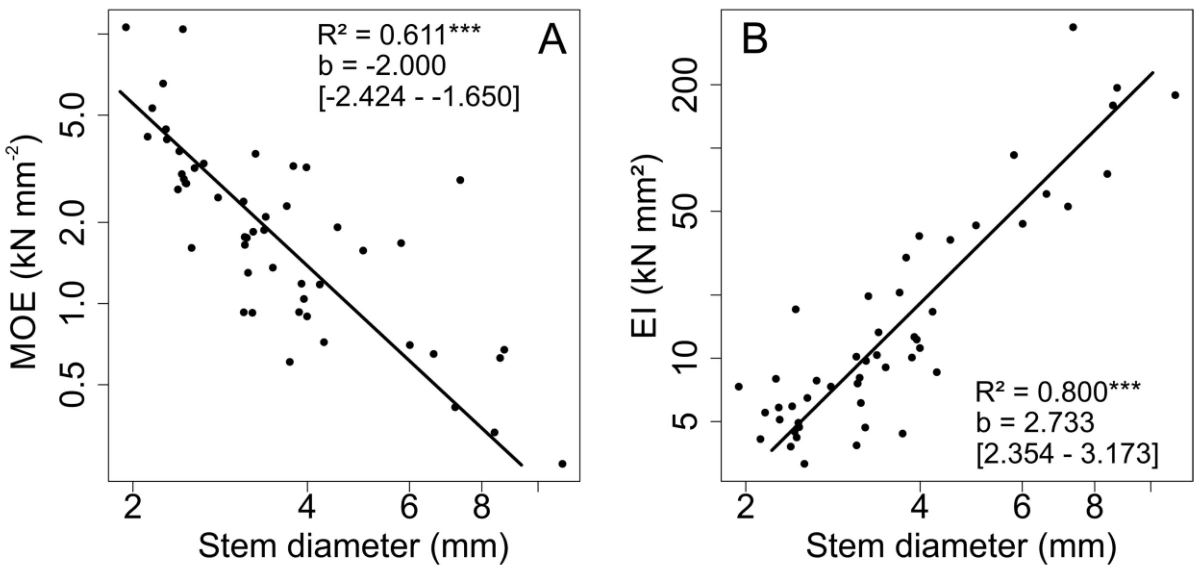

R² = 0.611***
b = -2.000
[-2.424 - -1.650]
A
MOE (kN mm-2)
5.0
2.0
1.0
0.5
2
4
6
8
Stem diameter (mm)
B
EI (kN mm²)
200
50
10
5
R² = 0.800***
b = 2.733
[2.354 - 3.173]
2
4
6
8
Stem diameter (mm)

Figure 5

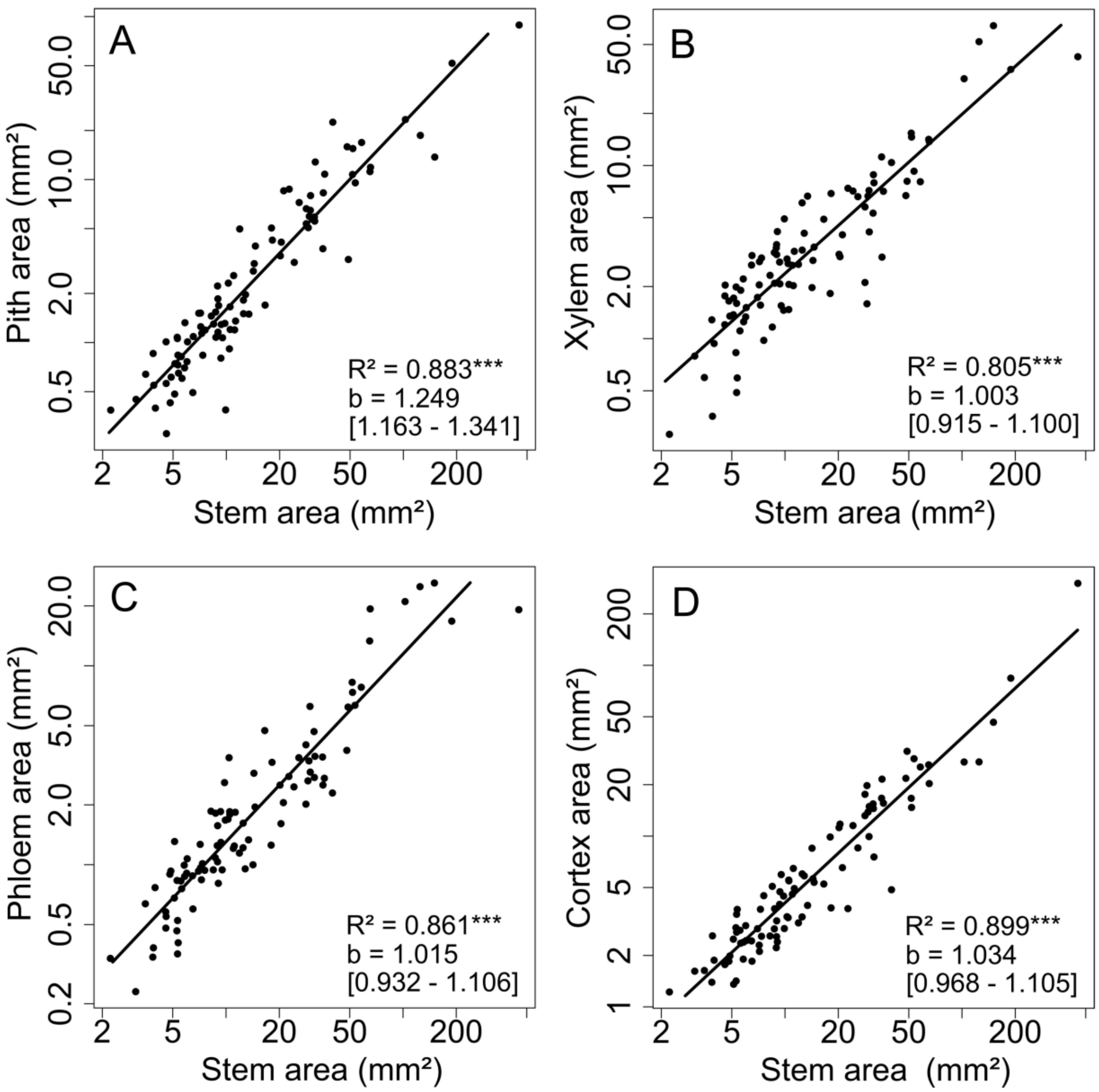
A
Pith area (mm²)
R² = 0.883***
b = 1.249
[1.163 - 1.341]
Stem area (mm²)
B
Xylem area (mm²)
R² = 0.805***
b = 1.003
[0.915 - 1.100]
Stem area (mm²)
C
Phloem area (mm²)
R² = 0.861***
b = 1.015
[0.932 - 1.106]
Stem area (mm²)
D
Cortex area (mm²)
R² = 0.899***
b = 1.034
[0.968 - 1.105]
Stem area (mm²)